Preliminary Study on Discharge Characteristics in a Capillary Discharge Based Pulsed Plasma Thruster for Small Satellites

IEPC-2017-433

Presented at the 35th International Electric Propulsion Conference
Georgia Institute of Technology • Atlanta, Georgia • USA
October 8 – 12, 2017

Le Cheng[1], Weidong Ding[2], Yanan Wang[3], Kaiyang Qian[4], Jiaqi Yan[5], Zhichuang Li[6] and Yue Li[7]
State Key Laboratory of Electrical Insulation and Power Equipment
&
Key Laboratory of Special Electrical Technology (Xi'an Jiaotong University), Ministry of Education
Xi'an Jiaotong University, No. 28, Xianning West Road, Xi'an, Shaanxi, 710049, P.R. China

Abstract: Compared to the traditional electromagnetic pulsed plasma thrusters(PPTs), the capillary discharge based PPTs, employing electrothermal plasma accelerating, have higher deposition energy efficiency in the discharge arc channel, which makes PPT a promising electric propulsion system for small satellites. In consideration of the huge necessity to obtain a great thrust efficiency performance under a low energy level (less than 10J), in this paper, the discharge characteristics in a capillary discharge based PPT have been investigated preliminarily. According to the typical discharge waveforms, the operation process in a discharge cycle was recognized. The influence of the initial charging voltage and cavity dimensions on equivalent plasma impedance, energy distribution and the energy deposition efficiency were also discussed. The results showed that lower initial voltage, longer cavity and smaller dimension lead to a larger equivalent plasma resistance higher energy deposition efficiency. Finally, the surface morphology of the capillary after 1000 shots was observed, which showed large nonuniformity of plasma jet in axial direction.

Nomenclature

C_0	=	main capacitance
C_1	=	trigger capacitance
ESR	=	equivalent series resistance
ESL	=	equivalent series inductance
EPR	=	equivalent plasma resistance
EPL	=	equivalent plasma inductance
η_{tran}	=	energy deposition efficiency
E_p	=	total deposited energy
R	=	resistance
L	=	inductance

[1] Graduate Student, Electrical Engineering, chengle_xjtu@foxmail.com.
[2] Professor, Electrical Engineering, wdding@mail.xjtu.edu.cn.
[3] Graduate Student, Electrical Engineering.
[4] Graduate Student, Electrical Engineering.
[5] Graduate Student, Electrical Engineering.
[6] Graduate Student, Electrical Engineering.
[7] Graduate Student, Electrical Engineering.

I. Introduction

PULSED plasma thrusters (PPTs) have been researched and developed widely since 1960s[1]. PPTs have many superior features: 1) simple structure and light weight by using solid fluorine plastics without complicated storage facilities. 2) generating high specific impulse under a low power level with a flexible autonomous control. 3) operating in a pulse form without preheating time. 4) providing thrust in μN scale that can be adjusted under constant specific impulse and thrust efficiency. Depending on above-mentioned advantages, PPTs have become one of the promising electric propulsion systems for small satellites in the field of attitude and orbit control[2].

Generally, based on the dominant plasma accelerating mechanism, PPTs are categorized into two types: electromagnetic PPTs (EM-PPTs) and electrothermal PPTs (ET-PPTs), the schematics of the two types are shown in Fig. 1. On account of the low performance in efficiency at specific impulse somewhat greater than 1000s, there is still a huge necessity to improve the thrust efficiency property of both the two types of PPTs under a low bank energy level[3].

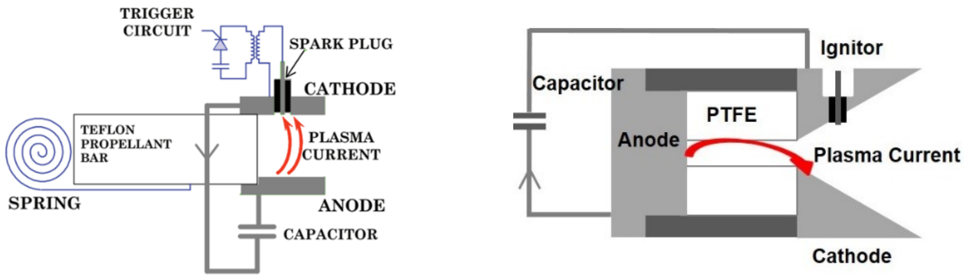

a) Schematic of EM-PPTs   b) Schematic of ET-PPTs

Figure 1. Schematics of two types of PPTs

According to the previous studies, since EM-PPTs utilizes electromagnetic force to accelerate charged particles of the plasma to produce thrust, late time ablation (LTA) and particulate emission are considered as the dominant factors of the low overall efficiency in EM-PPTs[4-5]. Differently, in a capillary discharge based PPT, the main discharge is ignited by initial plasma. Then a conductive path is set up between the anode and cathode. The discharge arc is constrained in the capillary tube and heat the propellant which dissociates and ionizes, then ablation plasma is ejected gas-dynamically to create thrust which is different from the mechanism of EM-PPTs. Thus, it means that the capillary discharge, a high-density plasma source, can accelerate charged and neutral particles sufficiently in a narrow cavity by electrothermal force, which provides a potential solution to enhance the thrust efficiency performance.

In the discharge process, the energy deposited in the arc plays an important role in ablation and plasma impedance. Plasma has great influence on the transfer efficiency of initial stored energy in turn. The proportion of the deposited energy limits the performance promotion of PPTs in a certain degree[6]. However, most of the previous research has mainly focused on the output thrust performance[7-10] with insufficient studies on the discharge characteristics, especially the energy deposition characteristic. In the interest of promoting and optimize the efficiency of low-power PPTs, an issue is to study the operation processes of the PPT from the view of discharge characteristics.

In this paper, an electrothermal PPT with novel capillary structure is designed and the discharge characteristics are investigated thoroughly. The discharge process was recognized according to the typical discharge waveforms. The equivalent circuit model and plasma impedance model were established. Meanwhile, the influence of the initial charging voltage and cavity dimensions on equivalent plasma impedance and energy deposition efficiency are also discussed. The results of the experiments in this paper lay a solid foundation for studying and optimizing the overall performance of electrothermal PPTs.

II. Experimental Apparatus

A. Configuration Description of Capillary-Based PPT DR-1

As is shown in Fig. 2, the electrothermal PPT DR-1 with a capillary structure contains a brass anode, a brass cathode nozzle, a capillary cavity made of polytetrafluoroethylene (PTFE) which is known as an excellent solid propellant in ablative thrusters for its best attribute of high overall performance[1], a PTFE outer sheath for insulation and sustaining the whole body and an igniter based on silicon carbide (SiC). There is a tight thread connection between the anode and the outer sheath to adapt to different lengths of the capillary cavities. The ignitor, including a high purity cylindrical tungsten electrode with diameter of 3.2mm and a semiconductor material bulk, is placed on the cathode nozzle. The tungsten electrode is selected for its excellent property of electro emission and erosion resistance. The semiconductor, which is made of SiC, zirconium dioxide (ZrO_2), aluminum oxide (Al_2O_3) and glass mixed in a particular proportion, is an essential of the ignitor[12]. The spark plug has an outstanding performance in producing initial charged particles, preventing carbon deposition, low porosity rate and low water absorption. As is tested in the experiment, there is no obvious erosion and carbon deposition on the surface of the semiconductor after ~10000 shots whilst the operation of the thruster shows great stability with barely several missing shots.

In this paper, the specific structure parameters of the PPT and the experimental conditions are shown in Table I.

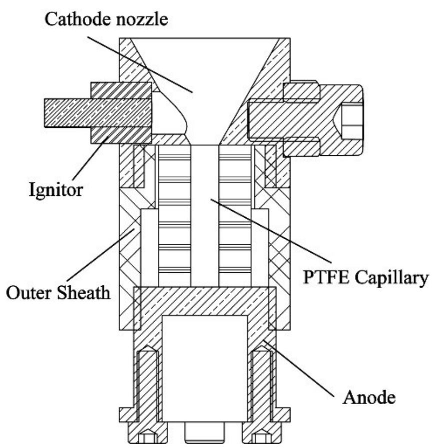

Figure 2. Schematic of PPT DR-1

Table I. Specific parameters and Experimental conditions

Items	Specifications
Cavity Diameter, mm	3, 4, 5
Cavity Length, mm	8, 9, 10,11,12
Nozzle Length, mm	10
Nozzle Half Angle, degree	20
Main Capacitance, μF	1.5
Charging voltage, kV	1.0 ~ 3.0
Initial Stored Energy, J	0.75 ~ 4.5
Ignition Energy, J	0.05

B. Experimental Setup

The capillary discharged based PPT experimental set up is depicted in Fig. 3. In this paper, the experiment platform main consists of two parts: a vacuum system and an electric parameters measuring system.

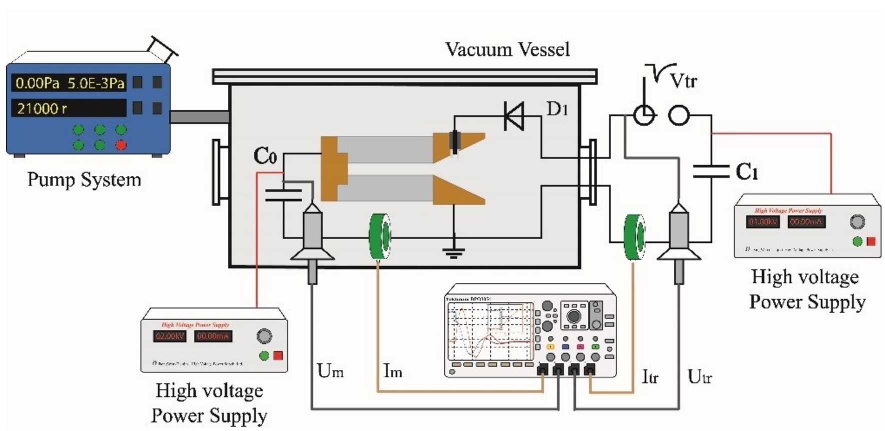

Figure 3. Schematic of the experimental setup

The vacuum system is composed of a stainless vacuum chamber with inner diameter of 0.7m and height of 0.45m, a sliding-vane rotary vacuum pump with a pumping speed of 48 L/s and a molecular pump with a pumping speed of 1500L/s. The pressure in the vacuum chamber is kept below 5×10^{-3}Pa during the thruster operation.

The discharge circuit contains the main circuit and the trigger circuit. In the main circuit, the main capacitor C_0 is in series connected with the PPT. The energy storage unit C_0 is selected for the EACO SDD (4000V, 1.5μF) with a low equivalent series resistance (ESR) to minimize the energy dissipation in the capacitor. Meanwhile, the transmission lines connected to the electrodes are made as short as possible to obtain a compact device to decline the parasitic inductance of the main circuit. The trigger circuit is composed of a trigger capacitor C_1, a trigatron switch, a blocking diode D_1, and the ignitor. The trigger circuit is used to generate a trigger voltage pulse and then make the surface of the ignition flashover to produce the initial plasma to ignite the main discharge. The capacitor C_1 is selected for the same type with C_0 while the specific parameters are 20000V and 0.1μF. Both of the C_0 and C_1 are charged to the operating voltages by dc power supplies. The charging voltage of C_0 is from 1.0kV to 3.0kV while that of C_1 is 1.0kV.

The trigatron switch is controlled by a high-voltage pulse generator based on IGBT and pulse transformer with adjustable frequency and amplitude. The blocking diode could reduce the energy consumption from the main discharge circuit to the trigger circuit.

To analyze the discharge characteristics of the capillary-based PPT systematically, the voltage waveforms on the C_0 and C_1 are measured through two high voltage probes Tek-6015A. Meanwhile, the current flowing through the main circuit and the trigger circuit are obtained by two Rogowski coils (Pearson 4997). All the waveforms are displayed and restored with a Tektronix DPO 3054 oscilloscope simultaneously.

C. Components Processing

The components of the experimental PPT would be polluted in the manufacturing process inevitably, including oil contaminated on the electrodes or the gases and water vapor absorbed in the propellant, which would change the experiment conditions and cause the inconsistency of discharges. Especially the loss of the gas absorbed in the propellant would affect the accuracy of measuring the mass loss[11]. It is necessary to process the components of the PPT before experiment. In this paper, the components were cleaned up in an ultrasonic cleaning machine for 30 minutes. After the contamination was removed, all the parts were moved into the vacuum drying oven. The oven was set with pressure below 0.1 Pa and temperature of 100 °C. The drying process last for 12 h. Consequently, the pretest mass measurement was performed as soon as the vacuum facility was vented in case of gases reabsorbing.

III. Results and Discussions

A. Analysis of the Typical Discharge Current and Voltage Waveforms

The experimental measured typical discharge current and voltage waveforms of the main discharge and the trigger discharge are shown in Fig. 4 where the main capacitor charging voltage is 3.0 kV. The length of the cavity is 11 mm and the diameter is 3 mm.

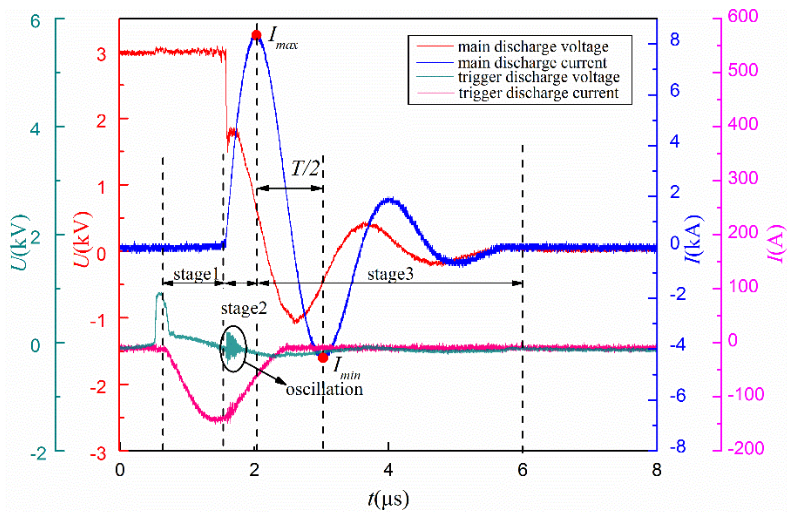

Figure 4. Typical discharge voltage and current waveforms obtained at the main voltage of 3.0 kV

As is shown in Fig. 4, a single discharge process of the capillary-based PPT consists of three stages: stage 1 of the ignitor flashover, stage 2 of the transition of the arc discharge and stage 3 of the main discharge.

Following a trigger signal sent to the IGBT, a high-voltage pulse is generated in the second winding of the pulse transform to make the trigatron switch conduct. Then a voltage pulse of which the rise time is about 90 ns and the amplitude is 900V is applied to the ignitor to make the semiconductor flashover. The amplitude of the trigger circuit current is 150A and the trigger discharge lasts for about 1.85 During the trigger discharge process, the voltage of the tungsten electrode occurs obvious oscillation. On one hand, the oscillation results from the electromagnetic interference (EMI) with the voltage measurement from the trigatron switch conducting. On the other hand, the change of the surface impedance of the ignitor would also lead to the instability of the trigger discharge.

In the stage 1, initial charged particles are produced to drift in the capillary cavity following the direction of the electric field lines. Afterwards, collisions occur between the initial plasma and the cavity wall to generate more charged particles by collision ionization. With the reduction of the insulation level of the capillary tube, the discharge process turns to the stage 2. The time duration of the stage 1 is defines as the trigger delay, which represents the time lag between generating initial plasma and igniting the discharge in the capillary. Under the typical experimental conditions, the trigger delay is about 0.91 μs. The factors that affects the trigger delay will be discussed in the further study.

Because of the dramatical drop of the resistance of the capillary cavity, the main capacitor, the anode and the cathode nozzle are in series connected with a transient discharge arc channel. There exists an obvious drop of the main capacitor voltage at the beginning of the stage 2. The drop voltage is about 1400V at the main charge voltage of 3.0 kV and the fall time is about 25 ns. According to the Burton and Turch[1], filaments and spot attachment exist at electrodes rather than a diffuse arc discharge channel during this stage.

In the stage 2, the main circuit current shows an increasing trend, in other words, the plasma resistance decreases synchronously, but still at a fairly high level. The temperature of the plasma channel is relatively low and the equilibrium vapor pressure on the surface of the wall has not been set up. The energy stored in C_0 is mainly used to heat the wall and ionize the molecule in this stage. Along with the temperature and the ionization degree of the plasma increasing, the plasma resistance achieves the minimal whilst the main discharge current reaches the maximum of 8.2 kA. Then, the discharge cycle steps into the stage 3, i.e., the quasi-stable main discharge.

In the main discharge stage, the main discharge current draws typical profile of dumped sine oscillation. The oscillation period of the main discharge is about 1.98 μs and the stage 3 lasts about 3.95 μs. The overall duration time of the discharge cycle from the beginning of ignitor flashover to the end of main discharge is about 5.35 μs. In the stage 3, most of the initial storage energy in C_0 is deposited in the plasma channel to dissociate and ionize the propellant. The discharge path is maintained by relative high-density plasma. Under the effect of gas-dynamic, plasma is accelerated and ejected to vacuum from the cathode nozzle.

B. Analysis of the Main Discharge Circuit and Equivalent Plasma Resistance

As the Fig. 4 shows, the main discharge current waveform in the capillary-based PPT features with an oscillation in the manner of a damped sine wave. Meanwhile, according to the electrical characteristics of the elements in the main circuit, the main discharge circuit can be simplified as an RLC circuit model generally. Fig. 5 depicts the schematic of the equivalent RLC circuit of PPT main discharge. C is the main capacitance. R_c and L_c are the equivalent series resistance (ESR) and equivalent series inductance (ESL) of the main capacitor, respectively. R_{tran1} and L_{tran1} are the resistance and inductance of transmission line to anode; R_{tran2} and L_{tran2} are the resistance and inductance of transmission line to cathode; and R_p and L_p are the equivalent plasma resistance (EPR) and the equivalent plasma inductance (EPL). $L_c + L_{tran1} + L_{tran2}$ and $R_c + R_{tran1} + R_{tran2}$ represent the parasitic inductor and the parasitic resistor in the main circuit, respectively, which are independent of the charging voltage and the capillary dimensions. The parasitic parameters were obtained by short-circuit discharge current waveform and the specific parameters are listed in Table II.

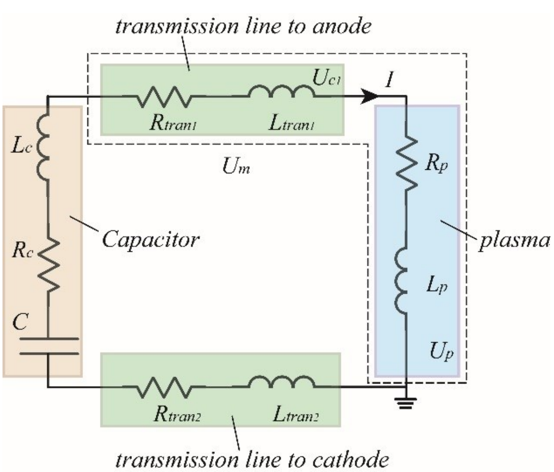

Figure 5. Schematic of the equivalent RLC circuit

Table II. Specific parameters of the parasitic elements

Parameters	Specifications
$L_c + L_{tran1} + L_{tran2}$, nH	50.5
$R_c + R_{tran1} + R_{tran2}$, mΩ	51.5

According to the experiment results, the main discharge circuit has been designed quite compact which would contribute to the storage energy deposited in the plasma channel rather than dissipated in the external circuit.

As is mentioned above, the main discharge of the capillary-based PPT can be regarded as an RLC discharge. Therefore, the expression of the main capacitor voltage and main discharge current can be represented as following equations:

$$U(t) = U_0 e^{-\delta t}\cos(\omega t) \tag{1}$$

$$I(t) = \frac{U_0}{\omega L_{eq}} e^{-\delta t}\sin(\omega t) \tag{3}$$

Where the U_0 is the initial voltage of the main capacitor, $\delta = R_{eq}/(2L_{eq})$ is the damping coefficient, $\omega = \sqrt{1/(L_{eq}C) - (R_{eq}/(2L_eq))^2}$ is the oscillation angular frequency, $R_{eq} = R_p + R_c + R_{tran1} + R_{tran2}$ and $L_{eq} = L_p + L_c + L_{tran1} + L_{tran2}$ are the equivalent resistance and the equivalent inductance of the main discharge circuit, respectively. It is worth noting that the second term in the oscillation angular frequency expression can be neglected due to the dominance of the first term. According to the Eq. (2), the R_{eq} and L_{eq} can be obtained from the following Eq. (3) and Eq. (4):

$$\left|\frac{I_{max}}{I_{min}}\right| = e^{\frac{R_{eq}T}{4L_{eq}}} \tag{3}$$

$$T = 2\pi\sqrt{1/(L_eqC)} \tag{4}$$

As is labeled is Fig .4, where the I_{max} and I_{min} represent the first and second peak current amplitude, respectively. The T is the oscillation period which is determined from the time interval between the Imax and Imin. With the calculation results of the R_{eq} and L_{eq}, the EPR and EPL can be derived from Eq. (3) and Eq. (4):

$$EPR = R_{eq} - R_c - R_{tran1} - R_{tran2} \tag{5}$$

$$EPL = L_{eq} - L_c - L_{tran1} - L_{tran2} \tag{6}$$

The specific values of the EPR and EPL with different main capacitor voltages and capillary dimensions and the relationships between the EPR and the energy deposition efficiency will be discussed in section C.

C. Energy Deposition Characteristics with Different Main Capacitor Voltages and Capillary Dimensions

In this section, the energy deposition characteristics in the plasma channel and the time dependent energy distribution mechanism are analyzed. In the experiment, the direct measurement of the voltage U_m contains the voltage across the transmission line to anode and the voltage across the plasma. With an LCR meter, the resistance R_{tran1} and the inductance L_{tran1} of the transmission line to anode are measured. The energy consumed on the R_{tran1} and the inductive energy storage are removed from the integral of the measured voltage and current data. Moreover, the measured U_m includes two parts of resistive component and inductive component. Correspondingly, the energy injected into the plasma channel was divided into one part of the joule heat energy and the other part of the magnetic field energy stored in the inductor. In this paper, the deposited energy refers to the joule heat energy deposited on the plasma resistance. Therefore, the deposited energy and the energy deposition efficiency are indicated as follows:

$$E_p\left(t_e\right) = \int_0^{t_e} U_m\left(t\right) I\left(t\right) dt - \int_0^{t_e} R_{tran1} I^2\left(t\right) - 1/2\left(L_p + L_{tran1}\right) I^2(t_e) \tag{7}$$

$$\eta_{tran} = E_p/(1/2CU_0^2) \tag{8}$$

Where the $E_p\left(t_e\right)$ is the pure resistive deposited energy in the plasma channel at the moment of t_e during the discharge process, η_{tran} and E_p are the energy deposition efficiency and the total deposited energy in a whole discharge cycle.

C-1 Energy deposition characteristics and equivalent plasma parameters with different main capacitor voltages

With a length of 8mm and a diameter of 3mm, the capillary discharge voltage waveforms and current waveforms under different main capacitor charging voltage are shown in Fig. 6. With the increase of the applied voltage, the drop of the voltage at the beginning of the stage 2 increases by nearly a linear trend whilst there is no significant change of the fall time. Meanwhile, the amplitude of the main discharge current and the duration of the main discharge increases. As discussed in the section A, the potential drop results from the voltage divide of the capillary impedance and the construction of the plasma channel. In this stage, the initial plasma channel impedance is mainly determined by the charged particles generated from the ignitor, i.e., by the energy stored in the trigger capacitor. In the experiments, the trigger energy remains a constant of 0.05J. That explains the phenomena of the linear growth of the potential drop and the nearly constant fall time.

According to the voltage and current waveforms in Fig. 6 and Eq. (7), the dependence of the energy distribution on the discharge time is shown in Fig. 7. It can be figured out that the energy deposited in the plasma resistance decreases with the increase in the charging voltage. As the discharge process develops, the amplitude of the voltage and current decline and the energy deposited plasma channel attenuates with it. Table III shows the deposited energy in the first two current oscillation periods accounts for the total deposited energy.

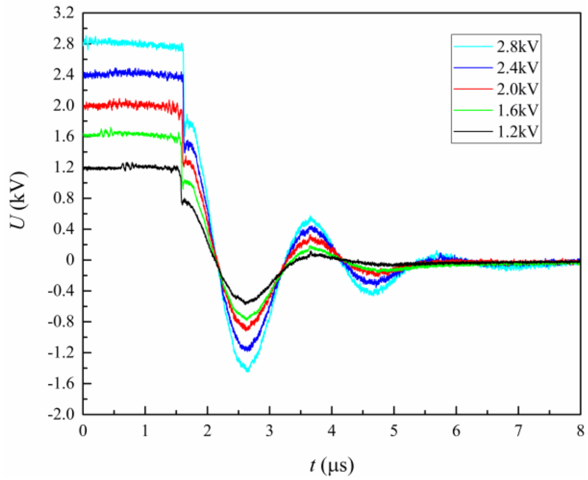

a) Discharge voltage waveforms

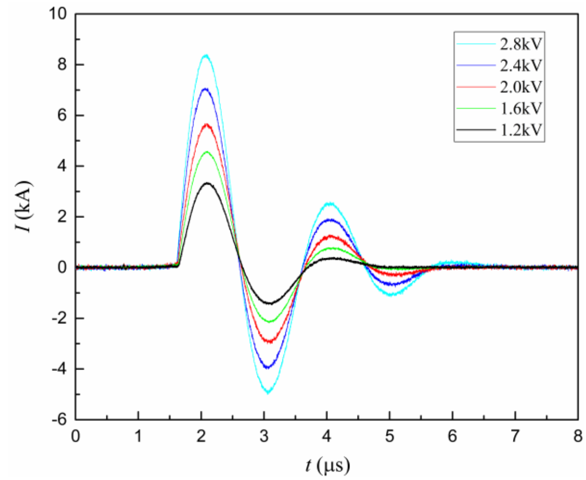

b) Discharge current waveforms

Figure 6. Discharge waveforms with different main voltages (*l* = 8mm and *d* = 3mm)

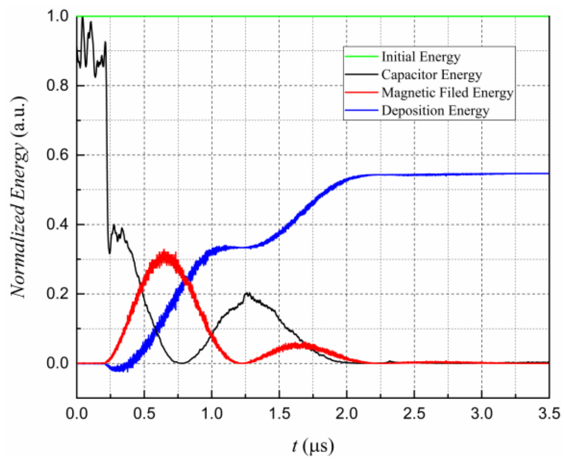

a) $U_0 = 1.2kV$

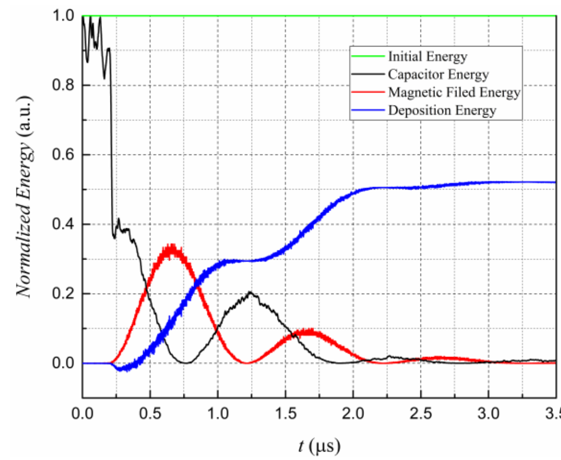

b) $U_0 = 2.0kV$

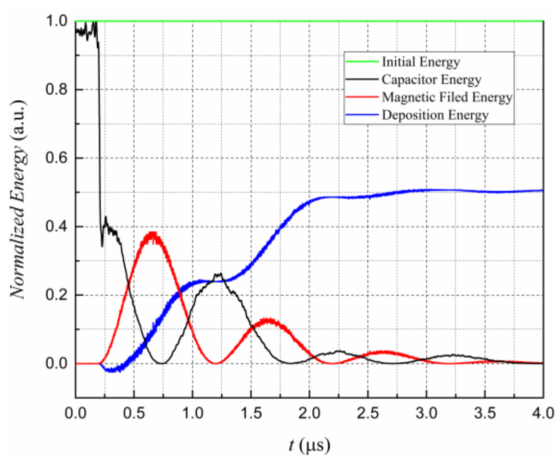

c) $U_0 = 2.8kV$

Figure 7. Effect of the main charging voltages on the energy distribution (*l* = 8mm and *d* = 3mm)

Table III. The deposited energy in each period accounts for the total deposited energy with different main voltages

Main charging voltage /kV	1.2	2.0	2.8
The energy deposition percentage in the first period /%	61.1	56.7	47.4
The energy deposition percentage in the second period /%	38.9	41.0	49.0
The energy deposition percentage in the first two periods /%	100	97.7	96.4

As the results shown in Table III, the proportion of the deposited energy in the first current oscillation period decreases from 61.1% to 47.4% with the increase of the main capacitor voltage. In the second period, the energy proportion improves from 38.9% to 49.0% while the deposited proportion in the first two oscillation periods declines from 100% to 96.4%. The results mean that the energy deposition process is mainly concentrated in the earlier stage of the discharge when the main charging voltage is low. Along with the main voltage increasing, the duration of the current oscillation extends, which results in a little part of the energy deposited in the plasma channel occurs in the later stage. However, the first two periods play a dominant role in the energy deposition and the thrust creation in the whole discharge process. In the later stage of the main discharge, the amplitude of the current is too small to ionize the neutral particles ablated from the propellant efficiently. Meanwhile, the vapor pressure is quite low and the velocity of the plasma bulk is negligible to generate valid specific impulse.

According to the Fig. 6 and Eq. (3) - (8), the equivalent plasma parameters, the total deposited energy and energy deposition efficiency are calculated. The results are shown in Table IV. With the main charging voltage increasing from 1.2 kV to 2.8 kV, the EPR decreases from 53.5 mΩ to 15.1 mΩ while the EPL decreases from 16.3 nH to 12.8 nH. Correspondingly, the energy deposition efficiency decreases from 54.78% to 50.52% since the efficiency can be expressed by Eq. (9) roughly:

$$\eta_{tran} \approx \frac{R_p}{R_p + R_c + R_{tran1} + R_{tran2}} \tag{8}$$

The decrease of the EPR leads to lower energy deposition efficiency at a higher main voltage, in other words, more energy is dissipated in the external circuit. Therefore, in order to promote the efficiency performance, the main discharge circuit should be designed as compact as possible.

Table IV. The equivalent plasma parameters and energy deposition parameters with different main voltages

Main charging voltage /kV	1.2	1.6	2.0	2.4	2.8
EPR /mΩ	53.5	43.9	31.5	21.9	15.1
EPL /nH	16.3	15.1	14.4	14.3	12.8
Deposited Energy /J	0.59	1.03	1.61	2.25	2.97
Energy Deposition Efficiency /%	54.78	53.83	53.60	52.14	50.52

C-2 Energy deposition characteristics and equivalent plasma parameters with different capillary lengths

Fig. 8 shows the discharge waveforms with different capillary lengths while the diameter of the capillary is 3mm and the applied main voltage is 2.0kV. As discussed in C-1, the drop voltage and the fall time at the beginning of the stage 2 are basically unchanged. The amplitude of the discharge current becomes lower and the duration of the main discharge becomes shorter with a longer length of the capillary. The energy distribution changing rule with different capillary lengths is shown in Fig. 9. The energy deposited in the plasma channel increases when the cavity gets long. Table V shows the deposited energy in the first two current oscillation periods accounts for the total deposited energy.

The calculation equivalent plasma parameters and the energy deposition efficiency with different capillary lengths are depicted in Table VI.

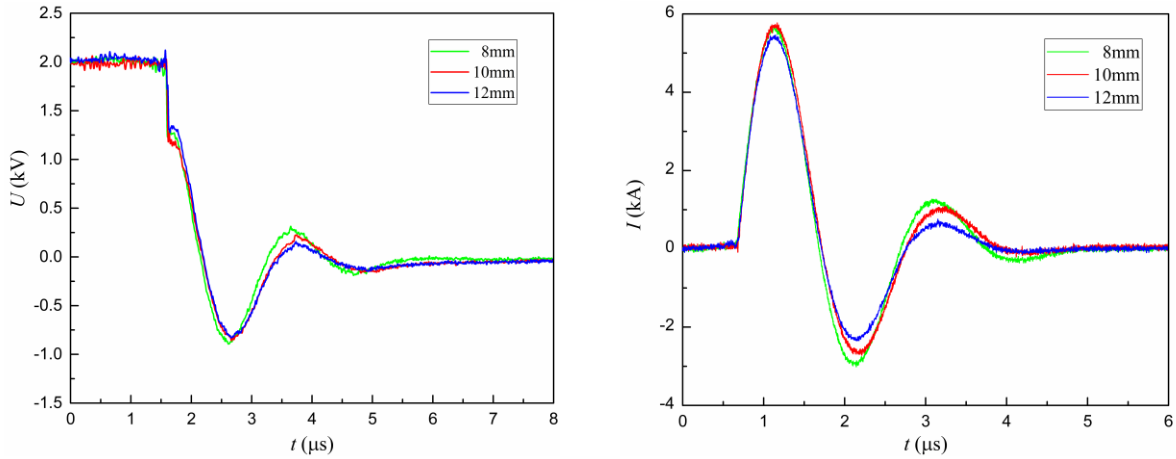

a) Discharge voltage waveforms b) Discharge current waveforms

Figure 8. Discharge waveforms with different capillary lengths (U_0 = 2.0kVand *d* = 3mm)

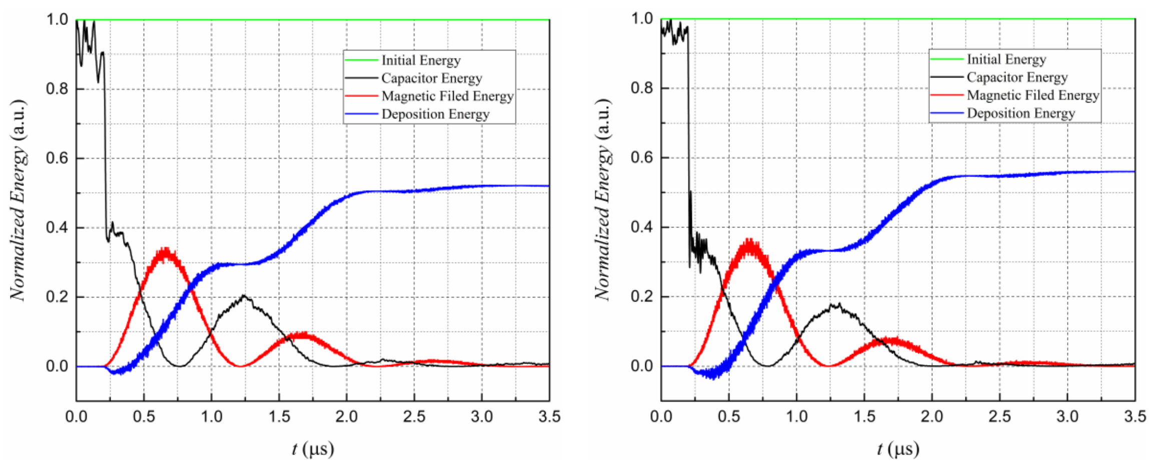

a) $l = 8mm$ b) $l = 10mm$

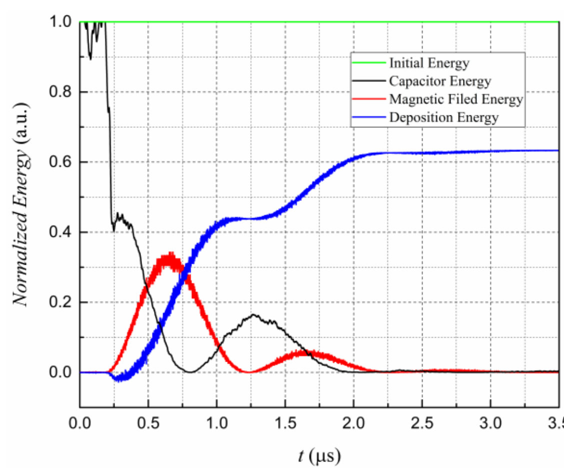

c) $l = 12mm$

Figure 9. Effect of the capillary length on the energy distribution (U_0 = 2.0kVand *d* = 3mm)

Table V. The deposited energy in each period accounts for the total deposited energy with different capillary lengths

Capillary length /mm	8.0	10.0	12.0
The energy deposition percentage in the first period /%	56.7	65.3	69.1
The energy deposition percentage in the second period /%	41.0	32.7	29.7
The energy deposition percentage in the first two periods /%	97.7	98.0	98.8

Table VI. The equivalent plasma parameters and energy deposition parameters with different capillary lengths

Capillary length /mm	8.0	10.0	12.0
EPR /mΩ	31.5	45.7	57.9
EPL /nH	14.4	17.2	13.2
Deposited Energy /J	1.61	1.72	1.92
Energy Deposition Efficiency /%	53.60	57.20	64.04

As Table V and Table VI shown, with the increase of the length of capillary cavity, the proportion of the deposited energy in the first current oscillation period increases from 56.7% to 69.1% while, the energy proportion decreases from 41.0% to 29.7% in the second period. Different from the regulation in Table III, the deposited proportion in the first two oscillation periods improves from 97.7% to 98.8% with the EPR increasing from 31.5 mΩ to 57.9 mΩ. The EPR is nearly proportional to the cavity length. A larger EPR makes the discharge current attenuate faster so that more proportion of the energy is deposited in the early stage of the discharge. Meanwhile, according to the Eq. (8), energy deposition efficiency is enhanced with a longer cavity because of the increasing EPR.

C-3 Energy deposition characteristics and equivalent plasma parameters with different capillary diameters

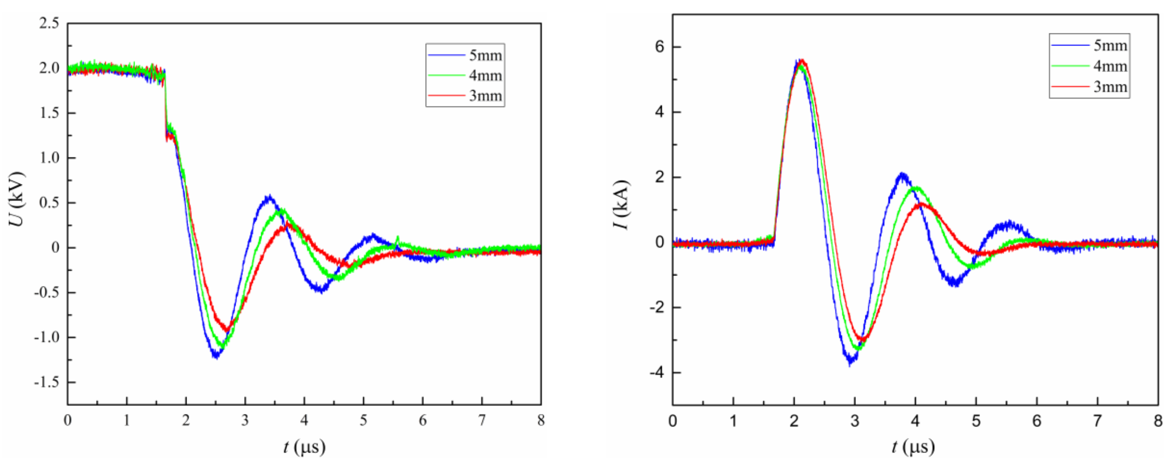

a) Discharge voltage waveforms
b) Discharge current waveforms

Figure 10. Discharge waveforms with different capillary diameters (U_0 = 2.0kVand l = 8mm)

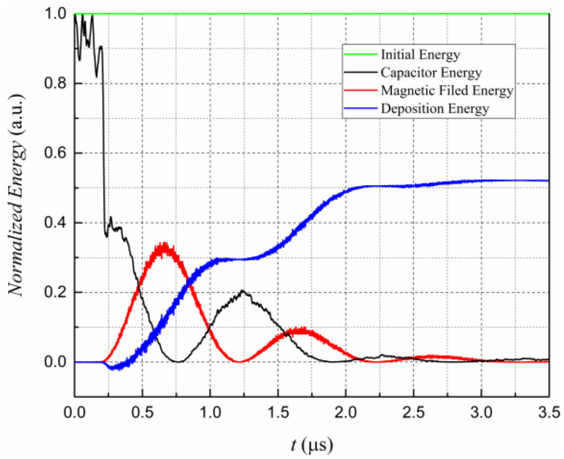

a) $d = 3mm$

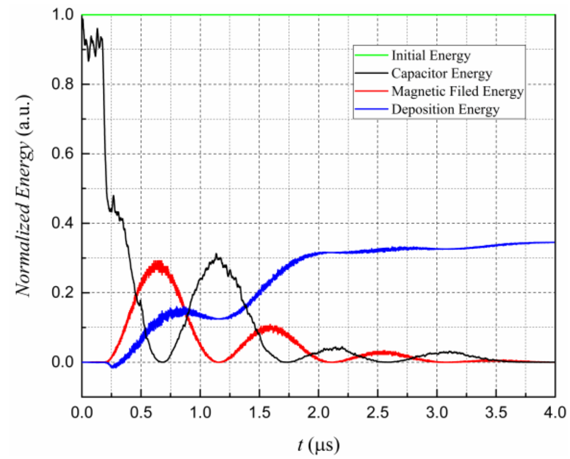

b) $d = 4mm$

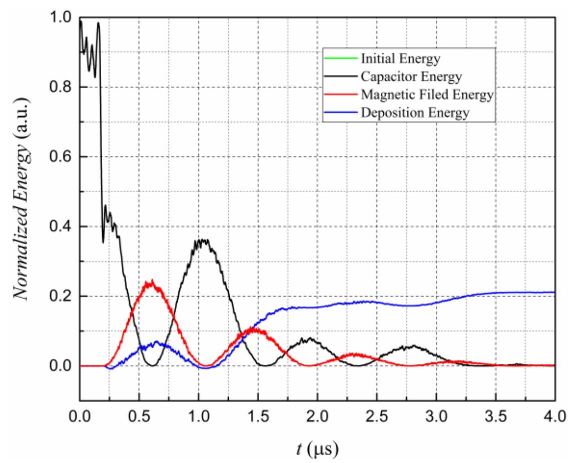

c) $d = 5mm$

Figure 11. Effect of the capillary diameter on the energy distribution (U_0 = 2.0kVand *l* = 8mm)

The discharge waveforms with different capillary diameters with an 8mm length of the capillary and a 2.0kV applied main voltage is shown in Fig. 11. Same as the regulation in C-1 and C-2, the process of the beginning of the stage 2 is similar with different cavity diameters. The amplitude of the discharge current increases and the oscillation period decreases when increasing the diameter. The energy distribution with different capillary diameters is shown in Fig. 11. The energy deposited in the plasma channel decreases when the cavity gets coarse. Table VII and Table VIII show the deposited energy in the first two current oscillation periods accounts for the total deposited energy and the calculation equivalent plasma parameters with different capillary diameters, respectively. The cavity with a smaller diameter is contributed to a larger EPR as well as the energy deposition efficiency.

Table VII. The deposited energy in each period accounts for the total deposited energy with different capillary diameters

Capillary diameter /mm	3.0	4.0	5.0
The energy deposition percent-age in the first period /%	56.7	36.8	31.3
The energy deposition percent-age in the second period /%	41.0	54.5	47.9
The energy deposition percent-age in the first two periods /%	97.7	91.3	79.2

The results in the Table VI and Table VIII seem that the energy deposition efficiency can be promoted with a longer and narrower cavity. However, increasing the length or decreasing the diameter of the capillary blindly are not always to improve the overall performance of PPT. On one side, the ignition of the PPT would be more difficult under a given trigger energy which is usually quite low compared to the main discharge energy when the capillary is too long or too narrrow. The initial plasma can not get into the cavity to generate secondary electron smoothly because of the blocking and absorption effect. On the other side, with the increase of the cavity length and the decrease of the cavity diameter, a negative effect on the velocity of the plasma would occurs because the increasing viscous resistance has an adverse influence on the plasma acceleration loss. Therefore, the optimum dimensions should be determined based on both the expected output performance of the capillary-based PPT and the energy deposition efficiency.

Table VIII. The equivalent plasma parameters and energy deposition parameters with different capillary diameters

Capillary diameter /mm	3.0	4.0	5.0
EPR /mΩ	31.5	13.2	11.0
EPL /nH	14.4	7.7	5.2
Deposited Energy /J	1.61	1.31	0.85
Energy Deposition Efficiency /%	53.60	35.20	21.09

IV.Conclusions

In this paper, the discharge characteristics in a low energy capillary discharge based PPT have been studied preliminarily by experiments. With the typical discharge waveforms, a single discharge process of the capillary-based PPT can be divided into three stages including the ignitor flashover, the transition of the arc discharge and the main discharge. The drop voltage at the beginning of the stage 2 is nearly proportional to the applied main voltage while independent of the capillary dimensions. Meanwhile, under a given trigger energy, the fall time is not significantly associated with the main charging voltage and capillary dimensions. An equivalent circuit model for the main discharge is set up. The parasitic parameters of the external circuit are obtained by short-circuit discharge experiment. The parasitic inductance is 50.5 nH and the parasitic resistance is 51.5 mΩ. The EPR, EPL, energy distribution regulation and energy deposition efficiency are closely related to the main charging voltage and capillary dimensions. With an applied main voltage increasing, the EPR decreases from 53.5 mΩ to 15.1 mΩ. Correspondingly, the energy deposition efficiency decreases from 54.78% to 50.52%. The increase of the cavity length and the decrease of the cavity diameter result in the increase of the EPR and consequently the increase of energy deposition efficiency. The energy deposited in the first two oscillation periods takes a dominant role in the total deposited energy of the whole discharge process. The energy deposition percentage in the first current oscillation period can be promoted with a lower main voltage and a capillary with a larger length and a smaller diameter to take better advantage of high current amplitude in the first discharge period to generate and accelerate the plasma bulk.

References

[1]Burton, R. L., and Turchi, P. J., "Pulsed Plasma Thruster," Journal of Propulsion and Power, Vol. 14, No. 5, 1998, pp. 716-735

[2]Takagi, H., Ishii, Y., and Tahara, H., "Performance Enhancement of Electrothermal Pulsed Plasma Thrusters for Osaka Institute of Technology Small Satellite," *31st International Electric Propulsion Conference*, Paper IEPC-2009-254, Sep. 2009.

[3]Rysanek, Filip, and R. Burton., "Performance and Heat Loss of a Coaxial Teflon Pulsed Plasma Thruster," Urbana, 2001.

[4]Antonsen, E. L., Burton, R. L., Reed, G. A., and Spanjers, G. G., "Effects of Postpulse Surface Temperature on Micropulsed Plasma Thruster Operation," Journal of Propulsion and Power, Vol 21, No. 5, 2005, pp. 877-883.

[5]Schönherr, T., Komurasaki, K. and Herdrich, G., "Propellant Utilization Efficiency in a Pulsed Plasma Thruster," Journal of Propulsion & Power, Vol 29, No. 6, 2013, pp. 1478-1487

[6]Edamitsu, T., Asakura, H., Matsumoto, A., and Tahara, H., "Research and Development of a Pulsed Plasma Thruster in Osaka University," *29th International Electric Propulsion Conference*, Paper IEPC-2005-106, Oct. 2005.

[7]Edamitsu, T., and Tahara, H., "Performance measurement and flowfield calculation of an electrothermal pulsed plasma thruster with a propellant feeding mechanism," *29th International Electric Propulsion Conference*, Paper IEPC-2005-105, Oct. 2005.

[8]M. Lau, G., Herdrich, S., Fasoulas, and H.-P. Röser, "A thermal pulsed plasma thruster for microsatellite propulsion," *32nd International Electric Propulsion Conference*, Wiesbaden, Germany, Sep. 2011.

[9]Iio, J., Uezu, J., Fukushima, T. and Kamishima, Y., "Evaluation on Impulse Bit Characteristics of Pulsed Plasma Thruster by Single Impulse Measurement," *29th International Electric Propulsion Conference*, Princeton, NJ, 2005.

[10]S. S. Bushman and R. L. Burton, "Heating and plasma properties in a coaxial gasdynamic pulsed plasma thruster," *J. Propuls. Power*, Vol. 17, No. 5, 2001, pp. 959–966.

[11]T. E. Markusic, K. A. Polzin, E. Y. Choueiri, M. Keidar, I. D. Boyd, and N. Lepsetz, "Ablative Z-pinch pulsed plasma thruster," J. Propuls. Power, Vol. 21, No. 3, 2005, pp. 392–400.

[12]Aston, G., and Pless, L. C., "Ignitor Plug Operation in a Pulsed Plasma Thruster," J. Spacecraft, Vol. 19, No. 3, 1982, pp. 250–256.